The Validity of the Kirchhoff Approximation for the Scattering of Electromagnetic Waves from Dielectric, Doubly Periodic Surfaces

M. Franco[1,3,*], M. Barber[2,3], M. Maas[3], O. Bruno[4], F. Grings[3], and E. Calzetta[1,5]

[1] Universidad de Buenos Aires, Facultad de Ciencias Exactas y Naturales, Departamento de Física. Ciudad Universitaria, Int. Güiraldes 2160, Buenos Aires, CABA, C1428EGA, Argentina
[2] Universidad de Buenos Aires, Facultad de Ingeniería, Departamento de Física, Av. Paseo Colón 850, Buenos Aires, C1063ACV, Argentina
[3] CONICET-Universidad de Buenos Aires, Instituto de Astronomía y Física del Espacio (IAFE), Ciudad Universitaria, Av. Cantilo S/N, Buenos Aires, C1428ZAA, Argentina
[4] California Institute of Technology, Mathematics Dept. MS 217-51201 East California Blvd,. Pasadena, CA 91125
[5] CONICET-Instituto de Física de Buenos Aires (IFIBA). Buenos Aires, Argentina.
[*] Corresponding author: mfranco@iafe.uba.ar

Compiled November 6, 2017

The accuracy of the Kirchhoff Approximation (KA) for rough-surface electromagnetic wave scattering is studied by comparison with accurate numerical solutions in the context of three-dimensional dielectric surfaces. The Kirchhoff tangent-plane approximation is examined without resorting to the principle of stationary phase. In particular, it is shown that this additional assumption leads to zero cross-polarized backscattered power, but not the tangent-plane approximation itself. Extensive numerical results in the case of a bisinusoidal surface are presented for a wide range of problem parameters: height-to-period, wavelength, incidence angles and dielectric constants. In particular, this paper shows that the range of validity inherent in KA includes surfaces whose curvature is not only much smaller, but also comparable to the incident wavelength, with errors smaller than 5% in total reflectivity; thus presenting a detailed and reliable source for the validity of KA in a three-dimensional fully polarimetric formulation.

OCIS codes: (290.5880) Scattering, rough surfaces; (290.5870) Scattering, Rayleigh; (290.1350) Backscattering; (000.4430) Numerical approximation and analysis.

http://dx.doi.org/10.1364/ao.XX.XXXXXX

1. INTRODUCTION

This paper studies the accuracy of the Kirchhoff theory of rough-surface electromagnetic wave scattering in the context of three-dimensional double periodic dielectric surfaces [1, 2], with an emphasis in cross polarization and total reflectivity. The need to evaluate the scattering of electromagnetic fields by rough surfaces arises in many applications. For example, in the field of active and passive microwave remote sensing, the evaluation of backscattered power and emissivity of agricultural fields and oceanic surfaces is of crucial importance. In view of the widespread use of the Kirchhoff Approximation (KA) [3–15] this paper seeks to supplement existing error studies for this method, and to provide a detailed and reliable source for its validity.

Historically, comparisons of the predictions arising from use of the KA with those of numerical methods were carried out in the late 80's [16, 17] by resorting to numerical methods applicable in the context of periodic (two-dimensional) perfectly conducting surfaces. In spite of having provided a very significant insight into the nature of the KA, these classical studies contain several limitations. In particular, effects such as shadowing and multiple scattering, that are sources of error in the KA, can have a significantly different impact in three-dimensional configurations as compared to periodic two-dimensional cases [7, 12]. More significantly, such two-dimensional geometries do not include the possibility of mode conversions, that only takes place in fully vectorial three-dimensional configurations.

Three-dimensional double periodic dielectric profiles were studied in [1, 2, 18] in the context of brightness temperature for ocean surfaces. In [1] the scattered wave from a bi-periodic surface is obtained through a procedure based on Huygens' principle and a Fourier expansion of the surface profile, while in [2, 18] the tangential fields on the surface are computed under physical optics and are used as a part of a Monte Carlo procedure

for randomly rough surfaces. In all these works the focus is on the brightness temperature and therefore do not provide details on the cross-polarized signal in the backscattering direction.

As more advanced numerical methods for the scattering of rough surfaces were developed in the past decades [19, 20], comparisons of the predictions of various approximate models and numerical solutions is now possible in the more relevant context of three-dimensional configurations. Nevertheless, comparisons require highly accurate numerical solutions that can still be quite expensive to achieve for the case of three-dimensional configurations. In the context of bi-periodic dielectric surfaces, the high order perturbation method [19] provides the required accurate solutions that include, in particular, accurate cross-polarizations and reflectivities. Using that method, this contribution systematically explores the range of validity inherent in Kirchhoff's tangent plane approximation, under no additional simplifying assumptions, and as a function of the various parameters of the problem: the height-to-period ratio of the illuminated surface, the dielectric constant, the incidence and observation angles, and the wavelength of the illuminating radiation.

The Kirchhoff Approximation relies in the combination of Huygens principle together with the tangent-plane approximation (i.e. the assumption that the induced currents at a point can be expressed by that resulting from a local tangent plane approximation of the surface). In order to evaluate the scattered field integral in the far-zone by an analytic closed form expression, Kirchhoff's original contribution additionally employed the approximation now known as stationary phase. Since then, this further high-frequency approximation became customarily used by many authors in view of its analytic usefulness. This additional assumption leads, in particular, to zero cross-polarization in the backscattering direction [4, 11] (i.e. an incident wave with a given polarization will be reflected with the same polarization), a fact that limits the experimental usefulness of the overall approach. In this work we examine the accuracy of the Kirchhoff tangent-plane approximation itself, which will be referred to as the Kirchhoff Approximation (KA), without resorting to additional approximations. The full expression to the surface induced fields is kept, and the resulting far-field expression is evaluated numerically. In particular, the present paper helps to clarify the effect of the stationary phase approximation in different regards, specifically on the effect on cross-polarized backscattered power, which, while the stationary phase predicts zero power, this is sometimes incorrectly attributed to the KA itself. In fact, as it is shown in [21, 22] for randomly rough surfaces, non-zero depolarization in backscattering condition under KA is achieved if the currents induced on the surface are written at least up to second order in the surface derivatives and stationary phase approximation is avoided.

Likewise, errors in both co-polarization and cross-polarization components are examined in detail. These errors, however, arise not only from the local geometrical tangent plane assumption, but also from global effects due to the overall shape of the rough surface, such as multiple scattering and shadowing. These global errors become larger as the roughness or incidence angle increase, or as the frequency decreases. Multiple scattering limits the amount of power scattered at large (grazing) scattering angles whereas surface shadowing reduces the total power scattered by a factor related to the portion of the scattering area that is illuminated. In these regards, the classical validity condition for KA, which states that a radius of curvature much larger than the incident wavelength is necessary, is examined in this paper in the case of an isotropic bi-sinusoidal diffraction grating. The analysis shows that this condition is exceedingly restrictive.

The paper is organized as follows: in Section 2 we develop the scattering of a electromagnetic plane wave over periodic surfaces in terms of the periodic Green function and the induced currents on the surface. Then, in Section C we give the amplitude of these induced currents using the tangent plane or Kirchhoff Approximation (KA). As our main interest is study how accurate results the KA, we need a standard to the scattering problem. This is briefly developed in Section D, where is given an overview for Perturbation Theory (PT) based on Padé approximants [19]. Finally, comparisons between KA and PT are shown in Section 3 for several sets of surface parameters as for different illumination geometries or incident wavelength. Section 4 contains our final remarks.

2. PRELIMINARIES

A. Scattered field

We consider the problem of scattering of an electromagnetic plane wave of wavelength λ, impinging from free space onto a three dimensional bi-periodic surface with spatial frequencies L_x and L_y in two orthogonal directions, acting as interface between two media where dielectric constant is ε.

The incidence plane wave is characterized by its wavenumber $\mathbf{k}_i$ defined in terms of the polar and azimuthal angles θ_i and ϕ_i, respectively, as shown in Figure 1.

$$\begin{cases} k_{ix} = k\cos(\phi_i)\,\sin(\theta_i) \\ k_{iy} = k\sin(\phi_i)\,\sin(\theta_i) \\ k_{iz} = -k\cos(\theta_i), \end{cases}$$

where $k = 2\pi/\lambda$. In what follows, $\mathbf{k}_{i\perp}$ will denote the projection of $\mathbf{k}_i$ on the mean plane of the surface.

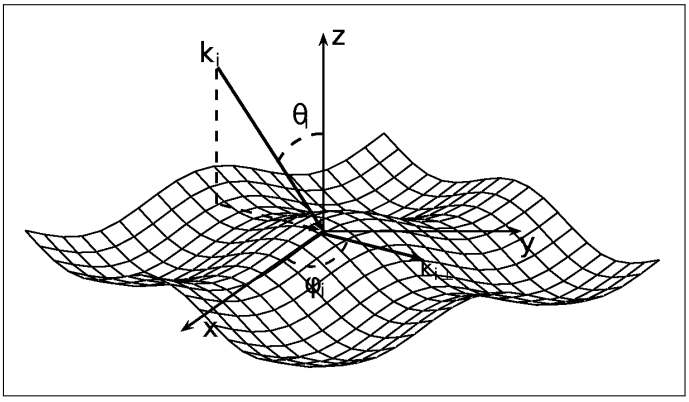

Fig. 1. Geometry of incident wave. $\mathbf{k}_{i\perp}$ is the component of $\mathbf{k}_i$ parallel to the mean plane of the surface.

The scattered field is a solution of Maxwell's equations, which can be written in integral form by resorting to the Huygens principle

$$\mathbf{E}^s(\mathbf{r}) = \int ds' \left\{ \nabla \times \bar{\bar{G}}(\mathbf{r},\mathbf{r}) \cdot \left[\hat{n}' \times \mathbf{E}(\mathbf{r}')\right] + \eta\, \bar{\bar{G}}(\mathbf{r},\mathbf{r}') \cdot \hat{n}' \times \mathbf{H}(\mathbf{r}') \right\}, \quad (1)$$

where $\mathbf{r}'$ is any point on the surface, $\bar{\bar{G}}(\mathbf{r},\mathbf{r}') = \left(\bar{\bar{I}} + \frac{\nabla\nabla}{k^2}\right) G(\mathbf{r},\mathbf{r}')$ is the dyadic Green, $G(\mathbf{r},\mathbf{r}')$ the scalar

free-space Green function and ∇ is the gradient with respect to $\mathbf{r}$; $\hat{n}'$ represents the normal to the surface at the surface point $\mathbf{r}'$, $\eta = \sqrt{\mu/\epsilon}$ is the impedance of the dielectric medium below the surface and $\mathbf{E}(\mathbf{r}')$ and $\mathbf{H}(\mathbf{r}')$ are the fields induced over the surface, which are still unknown variables. In equation (1) the integral is performed over the whole illuminated surface.

B. The Rayleigh Expansion for bi-periodic surfaces

For bi-periodic surfaces, the scattered can be expressed in terms of the Rayleigh Expansion [23] (see Appendix A for details)

$$\mathbf{E}_p^s(\mathbf{r}) = \sum_{n,m} e^{\imath(k_{nx}x + k_{my}y + k_{nmz}z)}\ \mathbf{B}_{nm}(\mathbf{k}_{nm}) \tag{2}$$

where the scattering directions $\mathbf{k}_{nm}$ are given by

$$\begin{cases} k_{nx} = k_{ix} + n\frac{2\pi}{L} \\ k_{my} = k_{iy} + m\frac{2\pi}{L} \\ k_{nmz} = \sqrt{k^2 - k_{nx}^2 - k_{my}^2}. \end{cases} \tag{3}$$

where $n, m \in \mathbb{Z}$ are known as the order of each mode.

It is clear that only a finite number of modes propagate away from the dielectric surface, i.e. the modes (n, m) such that k_{nmz} is real, as shown in Figure 2. The remaining modes decay exponentially. The transmitted modes can be expressed in a similar way, using the corresponding wavenumber for the dielectric medium ($k_t = \sqrt{\epsilon}\, k$) in which the transmitted wave propagates.

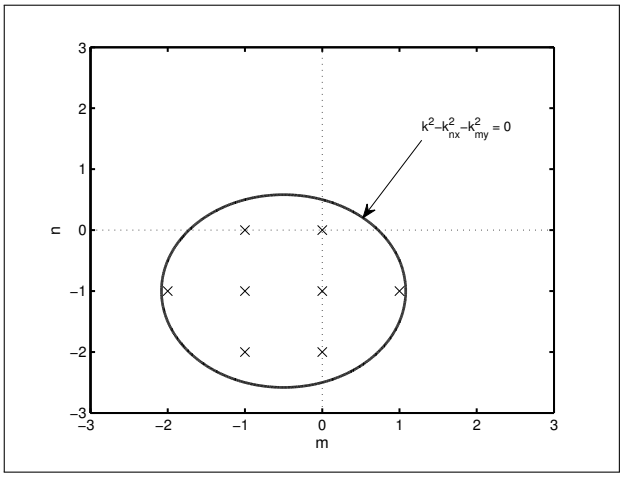

Fig. 2. Propagating modes (n,m) are defined by the integers (cross marks) laying within the contour level $k^2 - k_{nx}^2 - k_{my}^2 = 0$, whose shape is an ellipse. This contour is computed at $\theta_i = 45°$, $\phi_i = 63.4349°$, and $\frac{\lambda}{L} = 0.6325$, wherein eight propagating modes arose.

In the Rayleigh Expansion of equation 2, the amplitudes $\mathbf{B}_{nm}$ are given by

$$\mathbf{B}_{nm}(\mathbf{k}_{nm}) = \frac{1}{2\imath k_{nmz}} \frac{1}{L_x L_y} \int_{-L_x/2}^{L_x/2} dx' \int_{-L_y/2}^{L_y/2} dy'\, \mathbf{F}_p(\mathbf{r}') \times \\ \times e^{-\imath(k_{nx}x' + k_{my}y' + k_{nmz}z(x',y'))}. \tag{4}$$

where we have expressed the (unknown) induced currents over the surface for a $\hat{p}$-polarized incident wave, by

$$\mathbf{F}_p(\mathbf{r}') = (\hat{v}_s\,\hat{v}_s + \hat{h}_s\,\hat{h}_s)\cdot\hat{n}' \times \mathbf{H}_p(\mathbf{r}') + \frac{1}{\eta}\hat{k}_s \times \\ \times (\hat{v}_s\,\hat{v}_s + \hat{h}_s\,\hat{h}_s)\cdot\hat{n}' \times \mathbf{E}_p(\mathbf{r}'). \tag{5}$$

and where $\left\{\hat{k}_s, \hat{h}_s, \hat{v}_s\right\}$ denotes the orthonormal basis consisting of the propagation direction $\hat{k}_s$ of each mode, and the corresponding horizontal and vertical polarizations $\hat{h}_s, \hat{v}_s$, respectively. For details, see Appendix A.

For the finitely many propagating modes, we define the surface efficiencies as

$$e_{nm} = \frac{k_{nmz}}{k_{00z}} |\mathbf{B}_{nm}|^2. \tag{6}$$

We note that $k_{00z} = |k_{iz}|$ and, for a flat surface, $e_{00} = R_p^2$ ($p = h$ or v), i.e. the efficiency is proportional to the Fresnel reflection coefficient as expected for a specular reflection. The reflectivity R is defined as the sum of the efficiencies for each scattered mode,

$$R = \sum_{(n,m)\in U} e_{nm}, \tag{7}$$

where U is the set of propagating modes. Similarly, the transmissivity T is defined over the set of propagating transmitted modes. In the case of lossless media, the emissivity ε (measured in passive remote sensing) is given by $\varepsilon = 1 - R$.

Backscattering modes are important within various application areas, such as active remote sensing. For a backscattering mode to exist, $k_{nx}^{(bs)} = -k_{ix}$ and $k_{ny}^{(bs)} = -k_{iy}$ must hold, where (bs) stands for backscattering configuration. Using (3), this implies that

$$\begin{cases} k_{ix} + n_{bs}\frac{2\pi}{L} = -k_{ix} \\ k_{iy} + m_{bs}\frac{2\pi}{L} = -k_{iy}, \end{cases} \tag{8}$$

where the mode (n_{bs}, m_{bs}) is directed towards $-\mathbf{k}_{nm}$.

C. Kirchhoff Approximation

A surface is considered to be sufficiently flat when its radius of curvature is much larger than the incident wavelength. In detail [5],

$$2\, R_C\, k\, \cos^3\theta_l \gg 1 \tag{9}$$

where R_C is the mean radius of curvature of the surface, k is the incident wavenumber ($k = 2\,\pi/\lambda$) and θ_l is the local incidence angle defined as $\cos\theta_l = -\hat{n}\cdot\hat{k}_i$.

For bisinusoidal surfaces of the kind

$$z(\mathbf{r}) = -\frac{h}{4}\left[\cos(\kappa_x\, x) + \cos(\kappa_y\, y)\right] \tag{10}$$

with $\kappa_x = 2\pi/L_x, \kappa_y = 2\pi/L_y$, as shown in the Appendix B, the Kirchhoff condition (9), when $\kappa_x = \kappa_y = 2\pi/L$, is reduced to

$$C = \frac{h}{L}\frac{\lambda}{L}\frac{\pi}{\cos^3\theta_i} \ll 1, \tag{11}$$

In Figure 3 we show the contour levels resulting from inequality (11) as a function of $\frac{\lambda}{L}$ and $\frac{h}{L}$, for an incidence angle $\theta_i = 45°$. Throughout this paper, $\frac{h}{L} = 0.2$ and $\frac{\lambda}{L} = 0.6325$ will be used as reference, up to which the Kirchhoff solution will compared with highly accurate numerical solutions. This reference point is depicted as a black diamond in Figure 3, and is well beyond the validity condition given by inequality (9).

To use the tangent plane approximation we define a local orthonormal system at each point of the surface $\left\{\hat{n}, \hat{t}, \hat{d}\right\}$, following [4, 11, 13], by

$$\begin{cases} \hat{n}(\mathbf{x}') = \frac{-z_x(\mathbf{x}')\,\hat{x} - z_y(\mathbf{x}')\,\hat{y} + \hat{z}}{\sqrt{z_x^2(\mathbf{x}') + z_y^2(\mathbf{x}') + 1}} \\ \hat{t}(\mathbf{x}') = \frac{\hat{k}_i \times \hat{n}(\mathbf{x}')}{|\hat{k}_i \times \hat{n}(\mathbf{x}')|} \\ d(\hat{\mathbf{x}}') = \hat{k}_i \times \hat{t}(\mathbf{x}'). \end{cases}$$

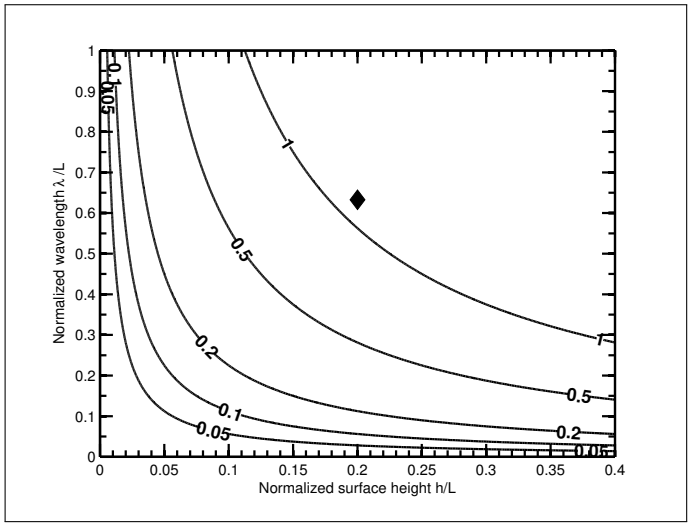

Fig. 3. Contour levels for Kirchhoff Approximation (KA) inequality applied to a doubly periodic bisinusoidal surface of period L in both directions. Incident radiation is at $\theta_i = 45°$. The smaller the level, the more accurate KA for describing the scattering from the surface.

The vectors $\hat{t}$ and $\hat{d}$ are the local decomposition of the perpendicular and parallel polarization with respect to the incidence plane defined by $\hat{k}_i$ and $\hat{n}$. The incident electric field can be decomposed into $\hat{t}$ (local TE mode) and $\hat{d}$ (local TM mode) components. Later, at each point of the surface we consider that the total electric field is the sum of the incident and the locally reflected, the latter proportional to the local Fresnel reflection coefficients $R_h(\mathbf{r}')$ (TE mode) or $R_v(\mathbf{r}')$ (TM mode). These coefficients are the usual ones, using the local incidence angle θ_l instead of the overall mean incidence angle θ_i.

Thus, for the TE mode as example, in (5) the tangent electric field induced at the point $\mathbf{r}'$, can be represented as [13]

$$\hat{n} \times \mathbf{E}_p(\mathbf{r}') = (\hat{n} \times \hat{t})(\hat{p} \cdot \hat{t})(1 + R_h(\mathbf{r}')), \tag{12}$$

and the corresponding magnetic field as

$$\hat{n} \times \mathbf{H}_p(\mathbf{r}') = -\frac{1}{\eta}\hat{t}(\hat{n} \cdot \hat{k}_i)(\hat{p} \cdot \hat{t})(1 - R_h(\mathbf{r}'). \tag{13}$$

Similar expressions can be given for the TM mode using the reciprocity property ($\mathbf{E} \to \mathbf{H}$, $\mathbf{H} \to -\mathbf{E}$ and $R_h \to R_v$).

Finally, considering the most general case where the incident field has both local components of polarization, the induced current on the surface under the Kirchhoff Approximation is then given by [11, 13]

$$\begin{aligned}\mathbf{F}_p^{KA}(\mathbf{r}') \quad &= \left[1 + z_x^2(\mathbf{r}') + z_y^2(\mathbf{r}')\right]^{1/2} \\ &\Big\{-(\hat{p} \cdot \hat{t})\,(\hat{n} \cdot \hat{k}_i)\,\hat{t}\,(1 - R_h(\mathbf{r}')) \\ &+(\hat{p} \cdot \hat{d})\,(\hat{n} \times \hat{t})\,(1 + R_v(\mathbf{r}')) \\ &+(\hat{p} \cdot \hat{t})\,(\hat{k}_s \times (\hat{n} \times \hat{t}))\,(1 + R_h(\mathbf{r}')) \\ &+(\hat{p} \cdot \hat{d})\,(\hat{n} \cdot \hat{k}_i)\,(\hat{k}_s \times \hat{t})\,(1 - R_v(\mathbf{r}'))\Big\}, \end{aligned} \tag{14}$$

Using this expressions, we will denote $\mathbf{E}_{qp}^s$ as the scattered field with polarization $\hat{q}$ that results from an incident wave with polarization $\hat{p}$. This is computed by taking the inner product between $\hat{q}$ and equation (2).

D. Perturbation theory

For comparison purposes, the amplitudes $\mathbf{B}_{nm}$ in (2) will be computed by using the numerical method put forth in [19], which will be referred to in this paper as the perturbation method. This method is based on boundary perturbations as depicted schematically in Figure 4, and is applicable to general bi-periodic surfaces, expressed in terms of their Fourier coefficients.

As shown in [19, 24], the scattered field of the surface $z(\mathbf{x})$ can be represented by a convergent power series on h. However valid, this power series can have a very small radius of convergence, so in order to obtain useful expressions, the method resorts to the use of Padé approximants. We will denote as the [U/V] Padé approximant of a function B_{nm}^l to the rational function whose Taylor series agrees with that of B_{nm}^l up to order U+V+1 [25]. In detail,

$$B_{nm}^l = \frac{a_0 + a_1 h + \cdots a_L h^U}{b_0 + b_1 h + \cdots b_M h^V} + \mathcal{O}(h^{U+V+1}) \tag{15}$$

where a's and b's coefficients are computed by solving a linear system on the coefficients of the power series representation of B_{nm}^l. Here, $B_{nm}^l (l = 1, 2, 3)$ are the components of the scattering amplitude vector $\mathbf{B}_{nm}(\mathbf{k}_{nm}) = [B_{nm}^1, B_{nm}^2, B_{nm}^3]$. In what follows, it will be assumed that $\mathrm{U} = \mathrm{V} = n_p$, where n_p will be the order of the Padé approximant.

The method of variation of boundaries has been demonstrated to be very accurate in numerous cases and has also been checked successfully against experimental data in optics [19, 26]. The method converges rapidly as the order of the Padé approximant is increased, and therefore, it will be used as benchmark to test the Kirchhoff Approximation.

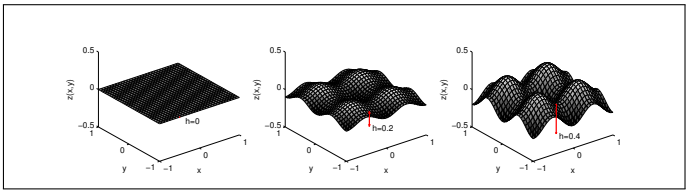

Fig. 4. A surface $z(\mathbf{r}) = -\frac{h}{4}\left[\cos(\kappa_x x) + \cos(\kappa_y y)\right]$ viewed as the perturbation of a smooth plane, from $h = 0$ to increasingly rougher parameterizations. It was proven in [24] that the electromagnetic field varies analytically with the parameter h, enabling a power series representation of the scattered field and Padé ressumation.

In order to assess the accuracy of the perturbation method for each scattered mode, we provide the following numerical experiment: for a fixed height-to-period ratio $\frac{h}{L}$, the order n_p of the Padé approximant is increased. As shown in Table 1, for a fixed illumination geometry $\theta_i = 45°$, $\phi_i = 63.4349°$, $\frac{\lambda}{L} = 0.6325$, vertically polarized radiation, and for fixed surface parameters $\frac{h}{L} = 0.20$, $\varepsilon = 36$, it is found errors in the reflected modes are better than 1×10^{-11} whenever $n_p \geq 14$. The order n_p is chosen by considering the conflicting requirements of both computing time and accuracy, specially for moderate values of $\frac{h}{L}$. This can be seen in Table 2, which contains an additional study for a much deeper surface with $\frac{h}{L} = 0.40$. Despite of the fact that accuracy gets poorer, it is still better than 1×10^{-3} (-30 dB error) for n_p larger than 14. Hence, in terms of accuracy, the perturbation solution can be regarded as a benchmark which the Kirchhoff solution can be compared to [19]. The computing time

Table 1. Convergence of the Perturbation method for each propagating mode, as the user-prescribed Padé approximant order n_p is increased, and elapsed time of computation. Simulation parameters are $\frac{h}{L} = 0.2$, and $\varepsilon = 36$.

Mode		Order n_p of Padé approximant		
n	m	6	10	14
-2	-1	3.4663045996e-04	3.4663079487e-04	3.4663079478e-04
-1	-2	7.1082895811e-04	7.1221054613e-04	7.1221054682e-04
-1	-1	1.5824016477e-02	1.5814203852e-02	1.5814203852e-02
-1	0	5.6868055231e-02	5.6857619817e-02	5.6857619810e-02
0	-2	6.8453781526e-03	6.8416409193e-03	6.8416409210e-03
0	-1	8.2355758510e-02	8.2336472323e-02	8.2336472334e-02
0	0	2.2870142288e-01	2.2871317645e-01	2.2871317646e-01
1	-1	3.2379974459e-03	3.2372545268e-03	3.2372545273e-03
time [min]		0.2	3.1	18.5

Table 2. Same as Table 2 for $\frac{h}{L} = 0.4$.

Mode		Order n_p of Padé approximant			
n	m	4	6	10	14
-2	-1	1,2074e-02	1.1971e-02	1.1977e-02	1.1977e-02
-1	-2	2,2946e-02	2.4449e-02	2.4414e-02	2.4415e-02
-1	-1	1,0251e-01	9.4817e-02	9.4590e-02	9.4585e-02
-1	0	7,7014e-02	7.4182e-02	7.4444e-02	7.4445e-02
0	-2	4,6445e-02	4.3652e-02	4.3601e-02	4.3601e-02
0	-1	8,0689e-02	7.7835e-02	7.8311e-02	7.8321e-02
0	0	3,6138e-02	3.7576e-02	3.7632e-02	3.7634e-02
1	-1	3,1400e-02	3.0911e-02	3.0545e-02	3.0546e-02
time [min]		0.03	0.2	2.9	17.8

for $n_p = 10$ and 14 in the configuration of Tables 1 and 2 are $\sim$ 3 and 18 min in a normal desktop computer (quad-core CPU at 3.40 GHz), respectively.

3. VALIDITY OF KIRCHHOFF APPROXIMATION

The present section analyzes the validity of tangent-plane approximation for varying values of the height-to-period ratio, dielectric constant ε, incidence angle θ_i, and wavelength-to-period ratio $\frac{\lambda}{L}$.

A. Dependence on surface height-to-period ratio

In this section, the second-order tangent plane approximation from Kirchhoff theory (K) is compared to the method of variation of boundaries from Perturbation (P) theory. In addition, results from the stationary phase approximation of the surface induced current is also shown. In the following, relative errors are computed as the ratio K/P. The simulation parameters are $\theta_i = 45°$, $\phi_i = 63.4349°$, $\frac{\lambda}{L} = 0.6325$, $L = 1.0$, and $\varepsilon = 9$. With this configuration, some power is backscattered: the backscattering mode (n_{bs}, m_{bs}) is (-1, -2).

The backscattered mode for vertically polarized (TM-case) incident radiation is shown in Figure 5 for varying surface height-to-period ratio. The comparison is done for co-polarized (pp) and cross-polarized (qp) efficiencies (upper panel), and performance is assessed as the ratio K/P for each $\frac{h}{L}$ (lower panel).

Figure 5 (left panel) shows how the efficiency $e_{-1,-2}$ corresponding to the co-polarized backscattering mode increases as the surface gets rougher as the height increases. The Kirchhoff prediction is slightly overestimated for larger heights, with a maximum relative error of 11% corresponding to $\frac{h}{L} \leq 0.20$.

On the other hand, the cross-polarized component of the backscattering mode (Figure 5, right panel) also increases with $\frac{h}{L}$. However, the Kirchhoff theory underestimates the backscattered efficiency since it is a first order prediction (single scattering) while depolarization effects are related to multiple scattering. Also, as expected, the tangent plane approximation degrades as $\frac{h}{L}$ increases, as shown in Figure 3. The stationary phase approximation yields zero cross-polarized backscattered power.

Notwithstanding this underestimation, it should be highlighted that in classical Kirchhoff Theory, where spatial derivatives in the surface induced currents are computed up to first order only, backscattered cross-polarized power is exactly zero. The fact that including the full expression for the induced currents yields a non-zero cross-polarized backscattered power, in agreement with [21, 22], where it is shown that for randomly rough surfaces depolarization under KA is obtained if the induced currents on the surface are written up to second order in surface derivatives.

The aforementioned remarks about the TM-case also apply to the backscattering mode for horizontally polarized (TE-case) incident radiation (Figure 6), where Kirchhoff agrees better than 11% for $\frac{h}{L} \leq 0.20$ for the co-polarized power. With the stationary phase approximation, the agreement is 2% poorer in the same range.

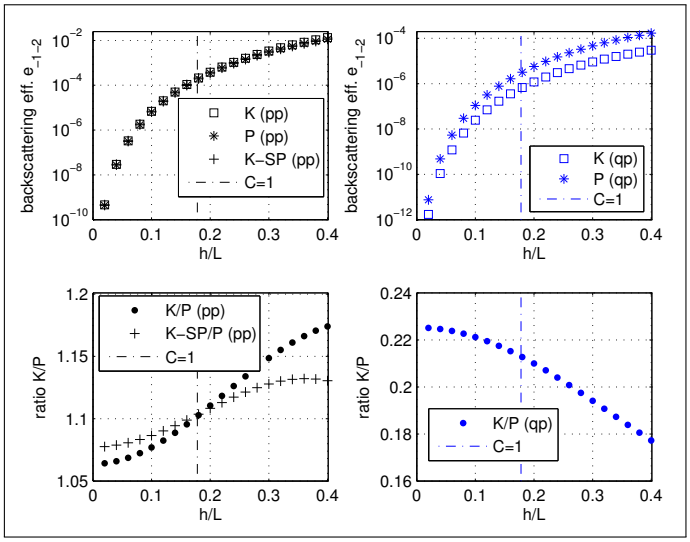

Fig. 5. Comparison of the backscattering efficiency $e_{\text{-1-2}}$ calculated from Kirchhoff (K) approximation, Kirchhoff approximation with stationary phase (K-SP), and from perturbation (P) theory with respect to the height perturbation parameter $\frac{h}{L}$. The dashed line corresponds to the left hand side of the validity condition (equation 11) to be equal to 1. The $[n_p/n_p]$ Padé approximant is computed for $n_p = 14$. Plane wave is vertically polarized (TM-case) impinging at $\theta_i = 45°$ and $\phi_i = 63.4349°$. Simulation parameters are $\frac{\lambda}{L} = 0.6325$, $L = 1.0$, and $\varepsilon = 9$. (Left panel) Co-polarized case (vv). (Right panel) Cross-polarized case (hv).

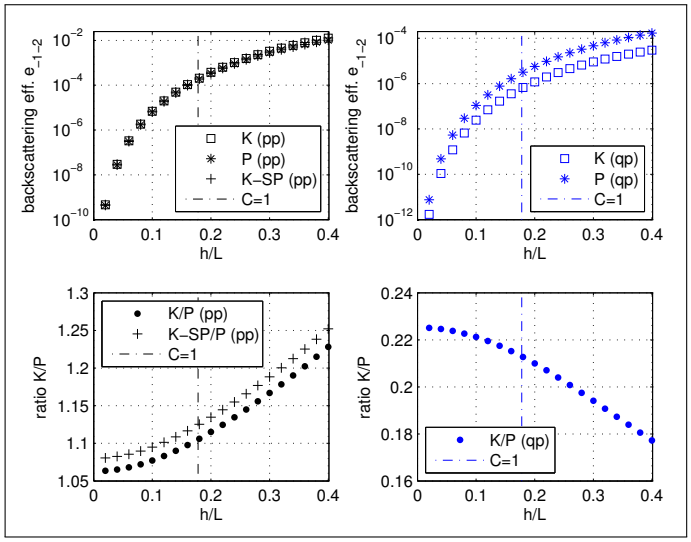

Fig. 6. The same as Figure 5 for a plane wave horizontally polarized (TE-case). (Left panel) Co-polarized case (hh). (Right panel) Cross-polarized case (vh).

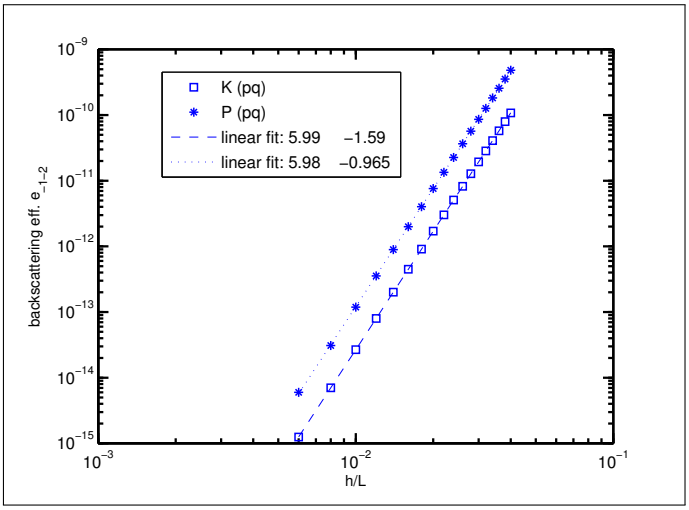

Fig. 7. Logarithmic scale plot depicting the dominant power in the computation of the cross polarized backscattering efficiency $e_{\text{-1-2}}$ by Kirchhoff and Perturbation theory for small values of the perturbation parameter $\frac{h}{L}$. The difference in intercepts depends on the dielectric constant (see Section B). Note that for such a range of small perturbation parameters, multiple scattering vanishes and energy is scattered by single scattering mechanisms only. Simulation parameters are the same as Figure 5.

In comparing both polarizations, it is found that the co-polarized efficiency for TM-case (i.e. vv) is greater than the one for TE-case (hh) in the backscattering configuration. Also, reciprocity theorem between TE- and TM-case establishes analytically that hv = vh at backscattering. This last statement is verified for $\frac{h}{L} \leq 0.2$ by plotting the induced currents (figures not shown) for hv and vh cases in a similar way as in [1] (Figures 8a to 8d therein).

Figure 7 shows the cross-polarized efficiencies on a logarithmic scale plot for values of $\frac{h}{L}$ in the range 0.006 to 0.040. The coefficients of the linear fit are shown in the legend. For such small perturbation parameters, multiple scattering vanishes and energy is scattered by single scattering mechanisms only. The $\left(\frac{h}{L}\right)^6$-dependence of the dominant power is due to the fact that the backscattered fields are scattered along the curvature of the 2D rough surface. It can be shown that for this particular surface the first four terms of the backscattered power vanish [27]. Therefore, the leading order in h for the backscattered radiation for this surface is h^6. The difference between the intercepts is due to different coefficients in the leading term of the induced currents for the cross-polarized efficiency. This difference is almost zero in the co-polarized efficiency (figure not shown), where the coefficients of the linear fit are (6.00,0.852) and (6.00,0.823) for Kirchhoff and Perturbation, respectively. This accounts for the excellent agreement showed in Figure 5 (left panel). It will be shown in Section B that the difference in intercepts depends on the dielectric constant.

It is worth mentioning that total reflectivity R, defined as in (7), can be seen as a measure of the overall error in the scattering process since it is includes all the propagating modes. In comparing to perturbation results for $\frac{h}{L} = 0.20$, relative errors as low as 1.2% for vertically and 2.7% for horizontally incident radiation are found.

Overall, the Kirchhoff Approximation performed well for both horizontal and vertical polarizations. Recall that the tangent-plane approximation accuracy is given by the inequality (9). As a reference, the vertical dashed lines in Figures 5 and 6 correspond to the case where the Kirchhoff condition's constant (C in left hand side of equation (11)) equals 1. The point $\frac{h}{L} = 0.20$ and $\frac{\lambda}{L} = 0.6325$ in the $(\frac{h}{L}, \frac{\lambda}{L})$-domain of Figure 3 is clearly beyond the expected validity range for the tangent-plane approximation to be accurate (level 0.1 or lower), and, nevertheless, very good results are obtained for such case (as it is discussed p.66 in [3] for 2D periodic profiles).

B. Dependence on dielectric constant

The accuracy of Kirchhoff approach is now assessed in terms of the dielectric constant ε of the surface. The simulation parameters used in this section are $\theta_i = 45^o$, $\phi_i = 63.4349^o$, $\frac{\lambda}{L} = 0.6325$, $L = 1$, and $\frac{h}{L} = 0.20$. Incident radiation is vertically polarized.

Backscattering efficiency is accurately predicted by the Kirchhoff theory for the co-polarized case, with relative errors below 12.5% for the range $\varepsilon = 1$ to $\varepsilon = 36$ (Figure 8, left panel). However, Kirchhoff approximation is unsuccessful in predicting the dependence of cross-polarized efficiency on dielectric constant (Figure 8, right panel). The non-monotonic behavior in K can be traced to a term of the kind $R_v(\varepsilon) + R_h(\varepsilon)$ in the Kirchhoff tangent fields of equation (14) after performing the dot product $\hat{q} \cdot \mathbf{F}_p(\mathbf{r}')$ and keeping the first non-zero power.

For lossless media (i.e. real-valued dielectric constant ε), absorptivity equals zero and energy balance implies that reflectivity R and transmissivity T satisfy $R + T = 1$. Moreover, as h increases from $h = 0$ (plane surface) onwards, power is redistributed from specular to non-specular modes. Hence, comparing total reflectivity R between K and P for different $\frac{h}{L}$ and ε might be useful in assessing the overall accuracy of the Kirchhoff Approximation. Figure 9a depicts relative error computed as $\frac{P-K}{P}$ for total reflectivity R as contour levels in the $(\varepsilon, \frac{h}{L})$-domain. Error is below 0.05 or 5% in the given range, being Kirchhoff reflectivity mostly underestimated (i.e. $P - K > 0$). This underestimation might be ascribed to the modes scattered off the

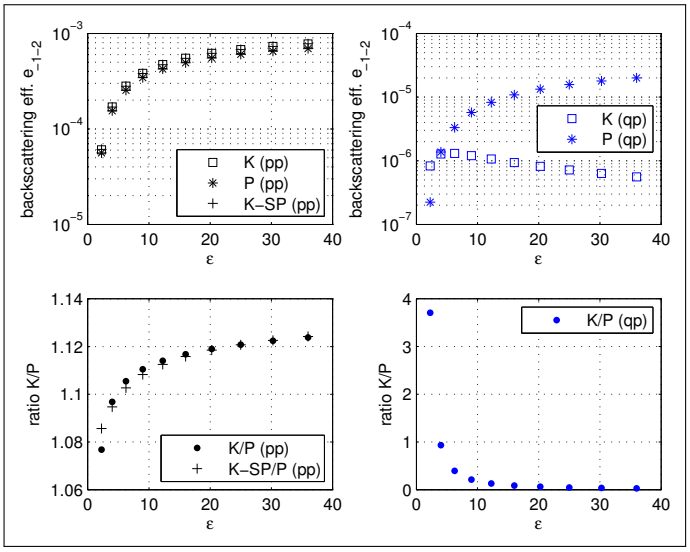

Fig. 8. Comparison of the backscattering efficiency $e_{\text{-}1\text{-}2}$ calculated from Kirchhoff (K) approximation, Kirchhoff approximation with stationary phase (K-SP), and from perturbation (P) theory with respect to the dielectric constant ε for a bisinusoidal surface of $\frac{h}{L} = 0.20$. The $[n_p/n_p]$ Padé approximant is computed for $n_p = 14$. Plane wave is vertically polarized (TM-case) impinging at $\theta_i = 45^o$ and $\phi_i = 63.4349^o$. Simulation parameters are $\frac{\lambda}{L} = 0.6325$, and $L = 1.0$. (Left panel) Co-polarized case (vv). (Right panel) Cross-polarized case (hv).

incidence plane with large angles, which are not accurately described in first order Kirchhoff theory. As $\frac{h}{L}$ increases, the contribution of non-specular modes to R increases markedly. The condition $C = 1$ given by the equation (11) is plotted as a vertical dashed line. For horizontally polarized incident radiation, a similar trend is found with errors below 5% (figure not shown).

Transmissivity can be assessed by means of $k_t = k\sqrt{\varepsilon}$, where k_t is the wavenumber for the transmitted radiation below the surface. This implies that wavelength λ_t in the transmitted medium is always greater than λ in the upper medium, weakening the inequality (9). Hence, a better accuracy for Kirchhoff theory for the transmitted modes is expected, as shown in Figure 9b, where the relative error is smaller than 0.8%.

In the case of horizontally polarized incident radiation, the magnitude of the transmissivity is smaller than in the vertically polarized case, so that differences between K and P have a more markedly impact on a ratio-based metric such as the relative error. Relative errors for transmissivity at horizontal polarization ranges from 0.5% to 6% (figure not shown).

C. Dependence on incidence angle

An assessment of the Kirchhoff Approximation error as a function of the incidence angle is now done in terms of the total reflectivity, which includes all the scattered modes.

Total reflectivity R as a function of the incidence angle θ_i for the Kirchhoff approach, perturbation method and Fresnel reflectivity for vertically and horizontally polarized incident radiation at $\phi_i = 63.4349^o$ is shown in Figure 10. Simulation parameters are $\varepsilon = 9$, $\frac{\lambda}{L} = 0.6325$, $L = 1.0$, and $\frac{h}{L} = 0.20$.

For vertically polarized incident radiation (Figure 10a), the Kirchhoff reflectivity agrees below 12% relative error to perturbation results up to the Brewster angle near $\tan^{-1}(\sqrt{\varepsilon}) \sim 71.57^o$, where the approximation degrades thereafter. For horizontal polarization (Figure 10b), the agreement is well until 60° with relative error below 17%. Dashed lines are the left hand side of equation (11) evaluated at the simulation parameters. Again, this values are far beyond the classical validity range of the Kirchhoff Approximation.

Table 3. Kirchhoff (K) and Perturbation (P) methods for several backscattering configurations θ_i- $\frac{\lambda}{L}$ from horizontally polarized (TE-case) incident radiation. The height-to-period ratio is $\frac{h}{L} = 0.20$. The remaining parameters are $\phi_i = 63.4349^o$, $\varepsilon = 9$, and $L = 1.0$. The last column states for the evaluation of equation (11).

Configuration		hh		vh		
θ_i	$\frac{\lambda}{L}$	K	P	K	P	C
20	0.3059	1.21E-02	1.19E-02	1.08E-06	4.46E-06	0.23
30	0.4472	2.94E-03	2.88E-03	1.05E-06	3.92E-06	0.43
40	0.5749	7.14E-04	6.69E-04	1.07E-06	6.36E-06	0.80
45	0.6325	3.75E-04	3.36E-04	1.20E-06	5.72E-06	1.12
50	0.6852	2.04E-04	1.63E-04	1.50E-06	7.01E-06	1.62

The discontinuities around $\theta_i = 15^o$, 23^o and 33^o in both polarizations are related to the fact that a number of propagating modes becomes non-propagating, as it is shown in the bottom panel of Figure 10. The energy carried by these modes is attenuated as the wave travels through the lossless media. For angles beyond 50°, in the present case, the change in the number of modes seem to have no effect in the continuity of the reflectivity R, since these modes have a low contribution to the total reflectivity.

D. Dependence on wavelength in Littrow configurations

This section performs an assessment of the Kirchhoff approach against the perturbation method for various values of the wavelength. In order to guarantee a backscattering mode exists (Littrow configuration), wavelength and incidence angle are varied pair-wise following equation (8), with the remaining parameters fixed at $\phi_i = 63.4349^o$, $\varepsilon = 9$, $\frac{h}{L} = 0.20$, and $L = 1.0$. In Table 3 Kirchhoff and perturbation methods for incident radiation at horizontal polarization are compared. Both co-polarized (pp) and cross-polarized (qp) backscattering modes are shown. Also, the Kirchhoff validity condition C given by equation (11) is shown. For the co-polarized efficiencies, an accuracy up two figures is reached provided Kirchhoff validity condition is less than one. Above this value, the accuracy gets poorer and it is conditioned mostly by the cubic power of the cosine of the incidence angle in the denominator of equation (11). For the cross-polarized case, the efficiencies follow the trend of the perturbation results up to $\theta_i = 40^o$. Again, reciprocity is verified at four figures on both methods. Similar results are found for vertically polarized incident radiation. In terms of the surface reflectivity R, an agreement up to 5.7% and 4.7% relative error is found for the configurations listed in Table 3 for both TE- and TM-cases respectively.

E. Dependence on wavelength in Bragg configurations

For moderate to large wavelength-to-period ratios, Bragg scattering occurs when L_x, $L_y \sim \frac{\lambda}{2\cos(\theta_i)}$. Under this condition, KA

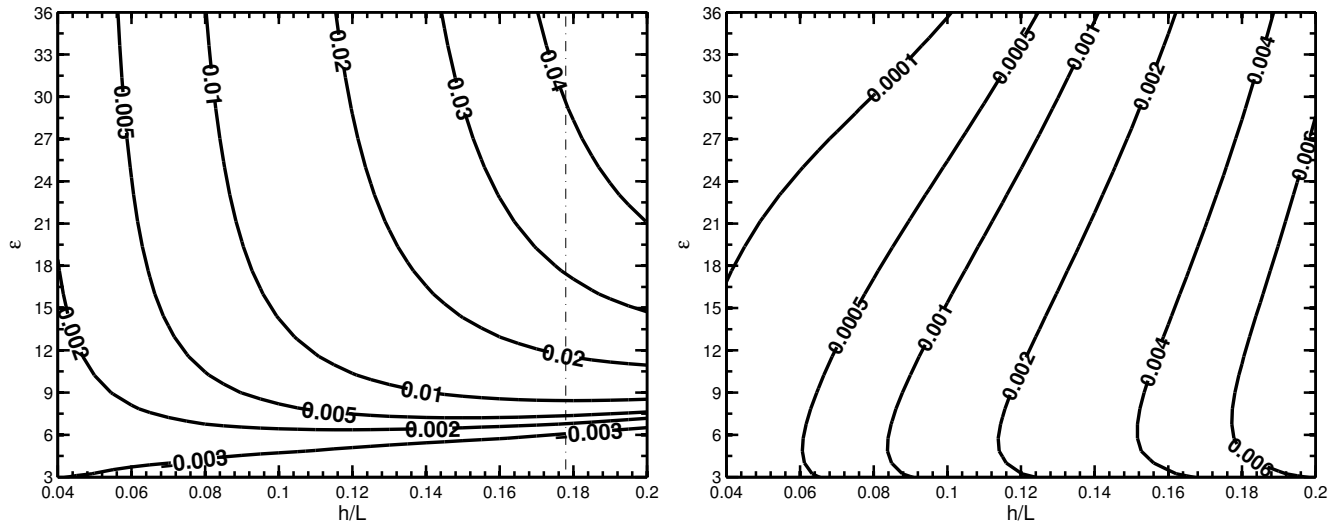

(a) Reflectivity R. **(b)** Transmissivity T.

Fig. 9. Contour levels for relative error $1 - \frac{K}{P}$ in the $(\frac{h}{L},\varepsilon)$-domain. Incident radiation is vertically polarized. The vertical dashed line states the left hand side of equation (11) to be equal to 1.

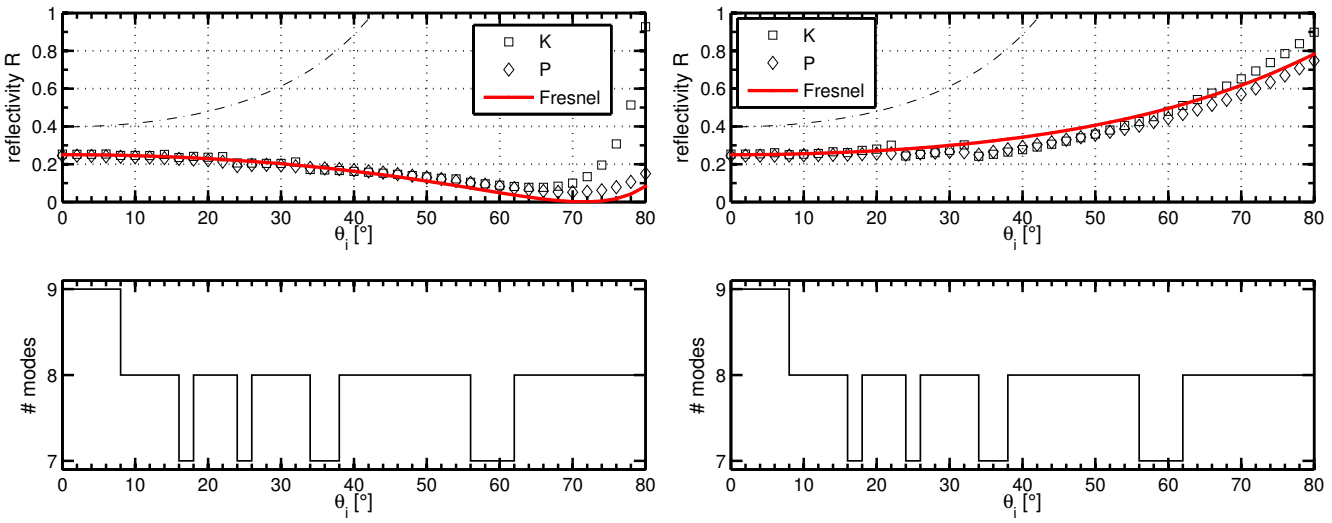

(a) Vertically polarized incident radiation. **(b)** Horizontally polarized incident radiation.

Fig. 10. Comparison of total reflectivity for Kirchhoff (K), perturbation (P) and Fresnel reflectivities (top panel) as a function of the incidence angle θ_i, at $\phi_i = 63.4349^o$. Simulation parameters are $\varepsilon = 9$, $\frac{\lambda}{L} = 0.6325$, $L = 1.0$, and $\frac{h}{L} = 0.20$. Dashed lines depict the left hand side of equation (11) evaluated at the simulation parameters. Number of propagating modes (bottom panel).

is expected to be only accurate for small ratios $\frac{h}{L}$ and small incidence angles θ_i, otherwise the Kirchhoff condition C will rapidly increase above one. Results comparing total reflectivity for several Bragg configurations are shown in Table 4 for both TE- and TM-case. Error in KA is as much as 2% for TE-case and less than 0.5% for TM-case. Also, it is found a marked effect of the incidence angle on the accuracy of KA in comparing to that of the wavelength-to-period ratio.

F. Dependence on amplitude and spatial period in two-scale surfaces

A more general surface involving two scales is of the kind

$$z(\mathbf{r}) = -\frac{h}{4}\left[a\cos(b\,\kappa\,x) + \cos(\kappa\,y)\right] \tag{16}$$

where parameters a and b accounts for some degree of heterogeneity between the x- and y-direction. Results comparing total reflectivity for varying a and b are summarized in Table 5.

As expected, Kirchhoff theory performance degrades as the spatial frequency increases. However, it is still accurate enough to yield errors around 12% and 15% for TE- and TM-case when $C \sim 1$. TE-case is found to be more accurate than TM-case indicating a lesser sensitivity to surface gradient.

Table 4. Total reflectivity R for several Bragg configurations and height-to-period ratios. Results are shown as the ratio of the Kirchhoff (K) to Perturbation (P) methods for TE- and TM-case. Kirchhoff condition C is also shown. The remaining parameters are $\phi_i = 0^o$, $\varepsilon = 9$, and $L = 1.0$.

K/P	$\frac{\lambda}{L} = 1.0000, \theta_i = 60^o$			$\frac{\lambda}{L} = 1.4142, \theta_i = 45^o$			$\frac{\lambda}{L} = 1.7321, \theta_i = 30^o$		
$\frac{h}{L}$	TE	TM	C	TE	TM	C	TE	TM	C
0.04	1.0033	0.9996	1.01	1.0022	1.0009	0.50	0.9998	1.0002	0.34
0.06	1.0074	0.9991	1.51	1.0050	1.0020	0.75	0.9996	1.0005	0.50
0.08	1.0132	0.9987	2.01	1.0089	1.0036	1.01	0.9992	1.0008	0.67
0.10	1.0206	0.9985	2.51	1.0139	1.0054	1.26	0.9987	1.0011	0.84

Table 5. Total reflectivity R for several two-scale configurations. Surface parameters a and b describing x-direction amplitude and spatial frequency are varied (see (16)). Results are shown as the ratio of the Kirchhoff (K) to Perturbation (P) methods for TE- and TM-case. Kirchhoff condition C computed for the surface given in (16) is also shown. The remaining parameters are $\theta_i = 45^o$, $\phi_i = 63.4349^o$, $\lambda = 0.6325$, $h = 0.05$, $\varepsilon = 9$, and $L = 1.0$.

K/P	$b = 1$			$b = 2$			$b = 3$		
a	TE	TM	C	TE	TM	C	TE	TM	C
0.2	0.9978	1.0020	0.09	1.1017	0.8642	0.13	1.1147	0.8493	0.21
0.5	0.9989	1.0007	0.11	1.1020	0.8640	0.23	1.1146	0.8525	0.43
1.0	1.0002	0.9981	0.15	1.1032	0.8628	0.40	1.1159	0.8600	0.86
1.5	1.0006	0.9947	0.19	1.1054	0.8604	0.59	1.1188	0.8687	1.36
2.0	1.0003	0.9907	0.23	1.1088	0.8557	0.80	1.1236	0.8756	1.99

4. CONCLUSIONS

The accuracy of the Kirchhoff Approximation (KA) for rough-surface electromagnetic wave scattering was studied in the context of three-dimensional dielectric surfaces and providing a detailed and reliable source for its validity. Classical error studies that have resorted to lower computational capabilities and, at the same time, low-order numerical methods, have only allowed to explore a limited set of problem parameters.

The main contribution of this paper is that the KA with a full expression in the surface currents is a good approximation, even for configurations close to the lower bound in the classical validity range, that expects KA to be reliable only when $R_C \gg \lambda$. Indeed, even in the cases in which $R_C \sim \lambda$, the KA calculates reasonably well the reflectivity and backscattered power for isotropic bi-sinusoidal diffraction gratings. This is relevant in the context of several application areas, where the classical condition hardly holds. In two-scale surfaces, where multiple-scattering and shadowing effect arise as relevant scattering mechanisms, the accuracy of KA is affected.

In the second place, the present paper contributes to reaffirm that depolarization can result by surface-scattering only, even when the tangent plane approximation is used [21, 22]. Indeed, it is a widespread misconception that zero cross polarization (hv) in backscattering direction occurs in KA. This paper showed that this is only due to further simplifying assumptions in addition to the Kirchhoff induced currents.

Regarding the absolute errors in the cross-polarized backscattered power, these are the same order of magnitude than the co-polarized errors. However, the relative errors can be larger in the case of low power signals. In fact, in the case of cross-polarized backscattering (hv), which is typically an order of magnitude smaller than the co-polarized case, the Kirchhoff Approximation provides, within its classical range of validity, the correct order of magnitude of the scattered signal. Underestimation in cross polarization is due to the fact that Kirchhoff Approximation reliably describes single scattering, where multiple scattering is neglected. Of course, when $C > 1$, KA leads to an overall large underestimation of the backscattered power. The larger errors with respect to the co-polarized case are related to the fact that the dominant power in the cross-polarized tangent fields is proportional to the sum of the Fresnel reflection coefficients.

This paper presented an extensive error analysis of the Kirchhoff tangent-plane approximation, for a wide range of parameters (height-to-period and wavelength-to-period ratios, dielectric constant, and incidence angle) and contributed to the understanding of one of the most fundamental analytic approximations in rough surface scattering, for the three-dimensional, fully vectorial, dielectric case. The present work facilitates further study involving more complex surfaces and other analytic approximations.

5. FUNDING INFORMATION

Work supported in part by CONICET, University of Buenos Aires and Agencia Nacional de Promoción Científica y Tecnológica (PICT-2014-0647).

A. APPENDIX: DEDUCTION OF RAYLEIGH EXPANSION

As we mentioned in Section 2B, the scattered field due to a periodic surface can be expressed in terms of discrete modes. In the followin we show how this result is obtained using just the far field approximation for the Green function.

Here on we will consider that the observation point is located at the Fraunhofer zone of diffraction, which is the case in the context of remote sensing, where the scattered field is calculated in the far field approximation. This fact allows us to deal with plane scattered waves rather than spherical ones. Then, the dyadic Green function takes a simple expression, because the differential operator is reduced to the observation direction: $\nabla \to \imath k\, \hat{k}_s$, then

$$\bar{\bar{G}}(\mathbf{r}, \mathbf{r}') = \left(\bar{\bar{I}} - \hat{k}_s\, \hat{k}_s\right) G(\mathbf{r}, \mathbf{r}') = \left(\hat{v}_s\, \hat{v}_s + \hat{h}_s\, \hat{h}_s\right) G(\mathbf{r}, \mathbf{r}'), \quad \textbf{(17)}$$

where we have used the fact that $\left\{\hat{k}_s, \hat{h}_s, \hat{v}_s\right\}$ forms an orthonormal basis. For the scalar Green function it is suitable to give its Weyl representation,

$$G(\mathbf{r}, \mathbf{r}') = \int \frac{d^2 k_\perp}{(2\pi)^2}\, e^{\imath \mathbf{k}_\perp \cdot (\mathbf{x} - \mathbf{x}')}\, \frac{e^{\imath k_z |z - z'(\mathbf{x}')|}}{2\imath k_z}, \quad \textbf{(18)}$$

where we have used that a point in the space is $\mathbf{r} = \mathbf{x} + z(\mathbf{x})\, \hat{z}$, and the wavenumber is written as $\mathbf{k} = \mathbf{k}_\perp + k_z \hat{z}$, being $k_z = \sqrt{k^2 - \mathbf{k}_\perp^2}$ with the condition $\mathbf{k}_\perp^2 < k^2$ for propagating modes.

If we assume that the incident wave has polarization $\hat{p}$ (either horizontal – TE mode or vertical – TM mode) and if we use the far field approximation for the Green function, the scattered field can be expressed as

$$\mathbf{E}_p^s(\mathbf{r}) = \int ds'\, \mathbf{F}_p(\mathbf{r}') \int \frac{d^2 k_\perp}{(2\pi)^2}\, e^{\imath \mathbf{k}_\perp \cdot (\mathbf{x} - \mathbf{x}')}\, \frac{e^{\imath k_z |z - z'(\mathbf{x}')|}}{2\imath k_z}, \quad \textbf{(19)}$$

where $\mathbf{F}_p(\mathbf{r}')$ represents the induced currents over the surface due to the incident wave with polarization $\hat{p}$,

$$\mathbf{F}_p(\mathbf{r}') = (\hat{v}_s\,\hat{v}_s + \hat{h}_s\,\hat{h}_s)\cdot\hat{n}'\times\mathbf{H}_p(\mathbf{r}') + \frac{1}{\eta}\hat{k}_s\times \times(\hat{v}_s\,\hat{v}_s + \hat{h}_s\,\hat{h}_s)\cdot\hat{n}'\times\mathbf{E}_p(\mathbf{r}'). \quad (20)$$

Now, we use the fact that the illuminated surface is periodic, and has discrete periodicity: $\mathbf{x}' \to \mathbf{x}' + \mathbf{L}_{nm}$, where $\mathbf{L}_{nm} = n\,L_x\,\hat{x} + m\,L_y\,\hat{y}$ for n and m integers. Then, instead of integrate over all the surface, we just integrate over one period and sum on all the (n,m) modes covering the total illuminated surface:

$$\mathbf{E}_p^s(\mathbf{r}) = \sum_{n,m=-\infty}^{\infty}\int_{L_x(n-1)/2}^{L_x(n+1)/2} dx' \int_{L_y(m-1)/2}^{L_y(m+1)/2} dy'\,\mathbf{F}_p(\mathbf{r}')\times \int \frac{d^2k_\perp}{(2\pi)^2}\,e^{\imath\mathbf{k}_\perp\cdot(\mathbf{x}-\mathbf{x}')}\,\frac{e^{\imath k_z|z-z'(\mathbf{x}')|}}{2\imath k_z}. \quad (21)$$

We can further exploit the periodicity of the surface observing that the double periodicity of the structure implies that the fields must be (n,m) quasi-periodic; i.e. they must verify $\mathbf{F}_p(\mathbf{r}'+\mathbf{L}_{nm}) = \mathbf{F}_p(\mathbf{r}')\,e^{\imath\,\mathbf{k}_{i\perp}\cdot\mathbf{L}_{nm}}$ [24]. Therefore, after some straightforward algebra,

$$\mathbf{E}_p^s(\mathbf{r}) = \sum_{n,m=-\infty}^{\infty}\int_{-L_x/2}^{L_x/2} dx' \int_{-L_y/2}^{L_y/2} dy'\,\mathbf{F}_p(\mathbf{r}')\times \times\int \frac{d^2k_\perp}{(2\pi)^2}\,e^{\imath\mathbf{k}_\perp\cdot(\mathbf{x}-\mathbf{x}')}\,\frac{e^{\imath k_z|z-z'(\mathbf{x}')|}}{2\imath k_z}\times e^{-\imath\,(k_x-k_{ix}n\,L_x)}\,e^{-\imath\,(k_y-k_{iy}m\,L_y)}, \quad (22)$$

where it was used the fact that $z'(\mathbf{x}'+\mathbf{L_{nm}}) = z'(\mathbf{x}')$ and $\mathbf{L}_{nm} = n\,L_x\,\hat{x} + m\,L_y\,\hat{y}$. The sum over the n,m index, which covers the surface through its periods, can be converted into a sum on Dirac delta functions. We just rewrite these sums as follows

$$\sum_{n=-\infty}^{\infty} e^{\imath\,n\,\alpha} = \sum_{n=-\infty}^{\infty} e^{\imath\,n\,\alpha}\underbrace{e^{-\imath n\,(2\pi n')}}_{1} = \sum_{n=-\infty}^{\infty} e^{\imath\,n\,(\alpha-2\pi n')}, \quad (23)$$

where n' can be any integer.

Now, we use the discrete Fourier transform: $\sum_n e^{\imath n\,(\alpha-\alpha')} = 2\pi\,\delta(\alpha-\alpha')$, but noting that $\alpha' = 2\pi n'$, which means we must sum over all the possible n'. Then, we have an infinite series of Dirac delta functions (or a Dirac comb), resulting in

$$\sum_{n=-\infty}^{\infty} e^{\imath\,n\,\alpha} = \sum_{n'=-\infty}^{\infty}\delta(\alpha-2\pi n'). \quad (24)$$

Using the above result in expression (22), and recognizing α_x as $L_x(k_x-k_{ix})$ and α_y as $L_y(k_y-k_{iy})$, the scattered field simplifies to

$$\mathbf{E}_p^s(\mathbf{r}) = \sum_{n,m=-\infty}^{\infty}\int_{-L_x/2}^{L_x/2} dx' \int_{-L_y/2}^{L_y/2} dy'\,\mathbf{F}_p(\mathbf{r}')\times \times\int \frac{d^2k_\perp}{(2\pi)^2}\,e^{\imath\mathbf{k}_\perp\cdot(\mathbf{x}-\mathbf{x}')}\,\frac{e^{\imath k_z|z-z'(\mathbf{x}')|}}{2\imath k_z}\times \delta(L_x(k_x-k_{ix})-2n\pi)\,\delta(L_y(k_y-k_{iy})-2m\pi). \quad (25)$$

We see that the integrals of the Green function collapse to $k_x \to k_{nx} = \frac{2n\pi}{L_x} + k_{ix}$, $k_y \to k_{my} = \frac{2m\pi}{L_y} + k_{iy}$ and $k_{nmz} = \sqrt{k^2 - k_{nx}^2 - k_{my}^2}$ due to the Delta functions. Again, after some straightforward algebra, the scattered field results

$$\mathbf{E}_p^s(\mathbf{r}) = \sum_{n,m} e^{\imath(k_{nx}x + k_{my}y + k_{nmz}z)}\;\mathbf{B}_{nm}(\mathbf{k}_{nm}) \quad (26)$$

being the equation (2) of Section 2B and which is known as the Rayleigh expansion for the scattered modes [23].

The amplitude of the induced surface fields $\mathbf{B}_{nm}$ is

$$\mathbf{B}_{nm}(\mathbf{k}_{nm}) = \frac{1}{2\imath k_{nmz}}\frac{1}{L_xL_y}\int_{-L_x/2}^{L_x/2} dx' \int_{L_y/2}^{L_y/2} dy'\,\mathbf{F}_p(\mathbf{r}')\times \times e^{-\imath(k_{nx}\,x' + k_{my}\,y' + k_{nmz}\,z(x',y'))}. \quad (27)$$

The transmitted modes can be given in the same way, just using the wavenumber for the dielectric medium ($k_t = \sqrt{\epsilon}\,k$) in which the transmitted wave propagates.

At this point, it just remains to give a closed expression to $\mathbf{F}_p(\mathbf{r}')$ in equation (5). This is done through the Kirchhoff approximation developed in Section 2C where the equation (14) gives a explicit expression for the induced fields over the illuminated surface.

B. APPENDIX: RADIUS OF CURVATURE FOR BISINUSOIDAL SURFACES

For a deterministic surface, the radius of curvature is a function of its first and second derivatives, and it is defined by the inverse of its curvature $H(\mathbf{x})$,

$$H(\mathbf{r}) = \left[\left(1+z_y^2(\mathbf{r})\right)z_{xx}(\mathbf{r}) + \left(1+z_x^2(\mathbf{r})\right)z_{yy}(\mathbf{r}) - 2\,z_x(\mathbf{r})\,z_y(\mathbf{r})\,z_{xy}(\mathbf{r})\right]\times\left[1+z_x^2(\mathbf{r})+z_y^2(\mathbf{r})\right]^{-3/2} \quad (28)$$

being $z_i(\mathbf{r})$ and $z_{ij}(\mathbf{r})$ the first and second derivatives of the surface.

We want to give a expression for equation (9), the validity condition of Kirchhoff approximation. If we consider that the bisinusoidal surface has the same periodicity for both directions, $L_x = L_y = L$ (i.e. $\kappa_x = \kappa_y = \kappa$), the mean curvature $H(\mathbf{r})$ for these kind of surfaces is just

$$H(\mathbf{r}) = h\kappa^2\left[\cos(\kappa y)\left(16 + h^2\kappa^2\sin^2(\kappa x)\right) + \cos(\kappa x)\left(16 + h^2\kappa^2\sin^2(\kappa y)\right)\right]\left[16 + (h\,\kappa)^2\left(\sin^2(\kappa x) + \sin^2(\kappa y)\right)\right]^{-3/2}. \quad (29)$$

Then, the radius of curvature R_C of equation (9) is given by $R_C(\mathbf{r}) = \frac{1}{|H(\mathbf{r})|}$. We also need the local incidence angle at each point of this surface,

$$\cos\theta_l = -\hat{n}\cdot\hat{k}_i = \frac{4\cos(\theta_i) + h\,\kappa\sin(\theta_i)\left[\cos(\phi_i)\sin(\kappa x) + \sin(\phi_i)\sin(\kappa y)\right]}{\left[16 + (h\,\kappa)^2\left(\sin^2(\kappa x) + \sin^2(\kappa y)\right)\right]^{1/2}}.$$

First, we must note that the product $R_C\,\cos^3\theta_l$ simplifies the factor involving the square root that normalize the normal of the surface. Once this term is simplified, inequality (9) becomes

$$1 \ll 2\,\frac{2\pi}{\lambda}\,\frac{1}{h\kappa^2}\times$$

$$[4\cos(\theta_i) + h\,\kappa\sin(\theta_i)\,(\cos(\phi_i)\sin(\kappa x) + \sin(\phi_i)\sin(\kappa y))]^3$$
$$\left|\cos(\kappa y)\left(h^2k^2\sin^2(\kappa x) + 16\right) + \cos(\kappa x)\left(h^2\kappa^2\sin^2(\kappa y) + 16\right)\right|^{-1}$$

Next, using $\kappa = 2\pi/L$ and factorizing out the cosine of the incidence angle, the condition of validity results

$$1 \ll \frac{L^2}{\pi h\lambda}\cos^3(\theta_i) \times f(x,y)$$

being

$$f(x,y) = [4 + h\,k\tan(\theta_i)\,(\cos(\phi_i)\sin(kx) + \sin(\phi_i)\sin(ky))]^3$$
$$\left|\cos(ky)\left(h^2k^2\sin^2(kx) + 16\right) + \cos(kx)\left(h^2k^2\sin^2(ky) + 16\right)\right|^{-1}.$$

Finally, the validity condition for the Kirchhoff approximation is

$$\frac{\pi}{\cos^3(\theta_i)}\frac{\lambda}{L}\frac{h}{L} \ll f(x,y). \tag{30}$$

Inequality (30) involves the product between the normalized wavenumber $\frac{\lambda}{L}$ and surface height $\frac{h}{L}$. This product must be smaller than a function $f(x,y)$ which characterizes the radius of curvature of the surface. The function $f(x,y)$ has a global minimum greater than one in the range $\frac{h}{L} = 0.2$ and incidence angles $\theta_i = 45^o$ and $\phi_i = 63.4349^o$. This is easily demonstrated by plotting $f(x,y)$ within a period (figure not shown). Thus, for such as values, the expression (30) is always satisfied.

Considering the two-scale surface, the inequality (30) is modified just rewriting the function $f(x,y)$ and taking into account that the new function will be depend on a and b, the parameters that drive the roughness of the surface. Thus, for a surface given by (16) the validity condition for KA has the same expression than (30) but changing $f(x,y)$ by

$$f_{mr}(x,y;a,b) =$$
$$[4 + h\,\kappa\,\tan(\theta_i)\,(a\,b\,\cos(\phi_i)\sin(b\,\kappa\,x) + \sin(\phi_i)\sin(\kappa\,y))]^3$$
$$\left|\cos(\kappa\,y)\left(a^2h^2\kappa^2\sin^2(b\,\kappa\,x) + 16\right) + a\,b^2\,\cos(b\,\kappa\,x)\left(h^2\kappa^2\sin^2(\kappa\,y) + 16\right)\right|^{-1}.$$

Again, the new inequality can be easily checked plotting within a period the ratio between the constant and the function. For instance, taking $h = 0.05$m, varying b from $1/3$ to 1 and leaving the remaining of the parameters unchanged, the condition the multi-roughness surface is satisfied for most of the values used and reaching a maximum of one in some cases where KA is not expected to be valid.

REFERENCES

1. J. Johnson and R. Kong, "Scattering and thermal emission from a two dimensional periodic surface," Progress In Electromagnetics Research **15**, 303–333 (1997).
2. J. Johnson, "Higher order emission model study of bi-sinusoidal surface brightness temperatures," Progress In Electromagnetics Research **37**, 79–99 (2002).
3. P. Beckmann and A. Spizzichino, "The scattering of electromagnetic waves from rough surfaces," Norwood, MA, Artech House, Inc., 1987, 511 p. (1987).
4. F. T. Ulaby, R. K. Moore, and A. K. Fung, *Microwave remote sensing: active and passive*, vol. 2 (Addison-Wesley Reading, MA, 1981).
5. A. Fung and H. Eom, "Note on the kirchhoff rough surface solution in backscattering," Radio Science **16**, 299–302 (1981).
6. S. Chuang and J. Kong, "Wave scattering from a periodic dielectric surface for a general angle of incidence," Radio Science **17**, 545–557 (1982).
7. A. Wirgin, "Scattering from sinusoidal gratings: an evaluation of the kirchhoff approximation," JOSA **73**, 1028–1041 (1983).
8. R. Shin and J. Kong, "Scattering of electromagnetic waves from a randomly perturbed quasiperiodic surface," Journal of applied physics **56**, 10–21 (1984).
9. R. J. Papa and J. F. Lennon, "Conditions for the validity of physical optics in rough surface scattering," IEEE transactions on antennas and propagation **36**, 647–650 (1988).
10. M. E. Veysoglu, H. Yueh, R. Shin, and J. Kong, "Polarimetric passive remote sensing of periodic surfaces," Journal of Electromagnetic Waves and Applications **5**, 267–280 (1991).
11. A. K. Fung, Z. Li, and K.-S. Chen, "Backscattering from a randomly rough dielectric surface," IEEE Transactions on Geoscience and remote sensing **30**, 356–369 (1992).
12. A. Gasiewski and D. Kunkee, "Polarized microwave emission from water waves," Radio Science **29**, 1449–1466 (1994).
13. L. Tsang and J. A. Kong, *Scattering of electromagnetic waves, advanced topics*, vol. 26 (John Wiley & Sons, 2004).
14. T. M. Elfouhaily and C.-A. Guérin, "A critical survey of approximate scattering wave theories from random rough surfaces," Waves in Random Media **14**, R1–R40 (2004).
15. A. A. Maradudin, *Light scattering and nanoscale surface roughness* (Springer Science & Business Media, 2010).
16. E. I. Thorsos, "The validity of the kirchhoff approximation for rough surface scattering using a gaussian roughness spectrum," The Journal of the Acoustical Society of America **83**, 78–92 (1988).
17. M. Chen and A. Fung, "A numerical study of the regions of validity of the kirchhoff and small-perturbation rough surface scattering models," Radio Science **23**, 163–170 (1988).
18. J. T. Johnson, R. T. Shin, J. A. Kong, L. Tsang, and K. Pak, "A numerical study of ocean polarimetric thermal emission," IEEE transactions on geoscience and remote sensing **37**, 8–20 (1999).
19. O. P. Bruno and F. Reitich, "Numerical solution of diffraction problems: a method of variation of boundaries. iii. doubly periodic gratings," J. Opt. Soc. Am. A **10**, 2551–2562 (1993).
20. L. Tsang, J. A. Kong, and K.-H. Ding, *Scattering of Electromagnetic Waves: Numerical Solutions* (Wiley, 2001).
21. J. Leader, "Bidirectional scattering of electromagnetic waves from rough surfaces," Journal of Applied Physics **42**, 4808–4816 (1971).
22. J. A. Holzer and C. Sung, "Scattering of electromagnetic waves from a rough surface. ii," Journal of Applied Physics **49**, 1002–1011 (1978).
23. R.Petit, M. Cadilhac, D. Maystre, R. McPhedran, M. Nevière, P. Vincent, G. Derrick, and L. Botten, *Electromagnetic theory of gratings* (Springer, 1980).
24. O. P. Bruno and F. Reitich, "Solution of a boundary value problem for the Helmholtz equation via variation of the boundary into the complex domain," Proceedings of the Royal Society of Edinburgh: Section A Mathematics **122**, 317–340 (1992).
25. G. A. Baker and P. Graves-Morris, *Padé approximants*, vol. 1 (Addison-Wesley, 1981).
26. O. P. Bruno and F. Reitich, "Numerical solution of diffraction problems: a method of variation of boundaries. ii. finitely conducting gratings, padé approximants, and singularities," J. Opt. Soc. Am. A **10**, 2307–2316 (1993).
27. J. T. Johnson, "Third-order small-perturbation method for scattering from dielectric rough surfaces," JOSA A **16**, 2720–2736 (1999).